Taylor & Francis
Taylor & Francis Group

Pharmaceutical Development and Technology

ISSN: (Print) (Online) Journal homepage: www.tandfonline.com/journals/iphd20

Targeted pH-responsive delivery of rosmarinic acid *via* phenylboronic acid functionalized mesoporous silica nanoparticles for liver and lung cancer therapy

Muhammad Kawish, Nimra Naz Siddiqui, Humera Jahan, Abdelbary Elhissi, Hina Zahid, Bushra Khatoon & Muhammad Raza Shah

To cite this article: Muhammad Kawish, Nimra Naz Siddiqui, Humera Jahan, Abdelbary Elhissi, Hina Zahid, Bushra Khatoon & Muhammad Raza Shah (2024) Targeted pH-responsive delivery of rosmarinic acid *via* phenylboronic acid functionalized mesoporous silica nanoparticles for liver and lung cancer therapy, Pharmaceutical Development and Technology, 29:6, 541-550, DOI: 10.1080/10837450.2024.2356210

To link to this article: https://doi.org/10.1080/10837450.2024.2356210

Published online: 24 May 2024.

PHARMACEUTICAL DEVELOPMENT AND TECHNOLOGY
2024, VOL. 29, NO. 6, 541–550
https://doi.org/10.1080/10837450.2024.2356210

Taylor & Francis
Taylor & Francis Group

RESEARCH ARTICLE

Targeted pH-responsive delivery of rosmarinic acid *via* phenylboronic acid functionalized mesoporous silica nanoparticles for liver and lung cancer therapy

Muhammad Kawish[a], Nimra Naz Siddiqui[b], Humera Jahan[b], Abdelbary Elhissi[c], Hina Zahid[d], Bushra Khatoon[a] and Muhammad Raza Shah[a]

[a]International Center for Chemical and Biological Sciences, H.E.J Research Institute of Chemistry, University of Karachi, Karachi, Pakistan; [b]Dr. Panjwani Center for Molecular Medicine and Drug Research, International Center for Chemical and Biological Sciences, University of Karachi, Karachi, Pakistan; [c]College of Pharmacy, QU Health, and Office of VP for Research and Graduate Studies, Qatar University, Doha, Qatar; [d]Department of Pharmaceutical Sciences, Dow University of Health Sciences Ojha Campus Karachi, Pakistan

ABSTRACT

Currently, chemotherapy is one of the most practiced approaches for the treatment of cancers. However, existing chemotherapeutic drugs have poor aqueous solubility, poor selectivity, higher systematic toxicity, and poor target accumulation. In this study, we designed and synthesized a boronic acid/ester-based pH-responsive nano-valve that specifically targets the microenvironment in cancer cells. The nano-valve comprises phenylboronic acid-coated mesoporous silica nanoparticles (B-MSN) loaded with polyphenolic compound Rosmarinic acid (ROS-B-MSN). The nano-valve was further coated with lignin (LIG) to achieve our desired LIG-ROS-BMSN nano-valve for targeted chemotherapy against Hep-G2 and NCI-H460 cell lines. The structure and properties of NPs were characterized by Fourier-transformed infrared spectroscopy (FTIR), Scanning Electron Microscopy (SEM) in combination with EDX, and Dynamic light scattering (DLS). The outcomes revealed that the designed LIG-ROS-BMSN were in the nanorange (144.1 ± 0.70 nm), had negative Zeta potential (-15.7 ± 0.46 mV) and had a nearly spherical morphology. *In vitro*, drug release investigations showed a controlled pH-dependent release profile under mild acidic conditions that could enhance the targeted chemotherapeutic response against cancer in mild acidic environments. The obtained LIG-ROS-BMSN nano valve achieved significantly lower IC_{50} values of (1.70 ± 0.01 μg/mL and 3.25 ± 0.14 μg/mL) against Hep-G2 and NCI-H460 cell lines as compared to ROS alone, which was (14.0 ± 0.7 μg/mL and 29.10 ± 0.25 μg/mL), respectively. The cellular morphology before and after treatment was further confirmed *via* inverted microscopy. The outcomes of the current study imply that our designed LIG-ROS-BMSN nanovalve is a potential carrier for cancer chemotherapeutics.

ARTICLE HISTORY
Received 1 November 2023
Revised 9 May 2024
Accepted 13 May 2024

KEYWORDS
Targeted chemotherapy; rosmarinic acid; pH-responsive drug delivery; boronic acid silica nanoparticles; liver cancer cells; lung cancer cells

1. Introduction

Cancer is currently regarded as a serious public health issue, and chemotherapy is one of the most effective anticancer strategies (Lavan et al. 2003; Cheng et al. 2017). Traditional drugs for chemotherapy operate primarily by interfering with DNA replication and mitosis to promote apoptosis in rapidly growing cancer cells, thereby limiting tumour growth and inhibiting metastatic Progression (Lavan et al. 2003; Torchilin 2014). On the other hand, these drugs have several drawbacks, including a short circulation life and low water solubility. A substantial number of chemotherapeutic drugs that are routinely delivered are harmful to healthy cells, demonstrating their non-selectivity (Petros and DeSimone 2010). Furthermore, chemotherapeutic drugs for the treatment of cells frequently result in multidrug resistance (MDR), which includes increased efflux, activation of nuclear DNA repair mechanisms, and changes in drug metabolism; these obstacles compromise the clinical effects of chemotherapeutic drugs (Elsabahy et al. 2015; Elsabahy and Wooley 2015). As a result, higher doses of chemotherapeutic agents are required to achieve the intended anticancer effect. Unfortunately, higher anticancer drug doses result in healthy tissue damage, hair loss, tiredness, infertility, and organ adverse effects.

The drawbacks of traditional chemotherapy have prompted the creation of an extensive range of nanoparticles for more effective and safer chemotherapeutic delivery. This includes organic (polymers (Kinoh et al. 2016), nonionic surfactants, graphene, and cellular membranes (Zhang et al. 2018)) and inorganic (iron, gold, silver, zinc, and silica) (Palanikumar et al. 2020). Mesoporous silica nanoparticles (MSNs) are a viable alternative support that has been widely employed due to their substantial pore volume, defined area, efficient biocompatibility, customizable structure, and thermal stability (Chan and Lin 2015; Wang et al. 2021). MSNs have high drug-loading efficiency due to their large and uniform pore size and can serve as an effective drug delivery mechanism for the administration of anticancer drugs (Li et al. 2020; Song et al. 2020). Furthermore, MSNs can be functionalized with molecular and polymeric moieties on the core to provide controlled drug delivery (Li et al. 2020). Accordingly, the exterior surfaces of MSN can be coated with switchable gatekeepers that respond to external stimuli such as light, pH, temperature, and antibodies, allowing therapeutic molecules to be delivered on demand .

Although cancer cells have lower extracellular (6.5–6.8) and intracellular pH (4.5–5.5) than normal tissues (7.2-7.4),

CONTACT Muhammad Raza Shah raza.shah@iccs.edu International Center for Chemical and Biological Sciences, H.E.J. Research Institute of Chemistry, University of Karachi, 75270 Karachi, Pakistan

pH-responsive drug delivery systems have attracted great interest (Volk et al. 1993). Based on our information, two types of methodologies were adopted to prepare pH-responsive systems. One is to functionalize acid-labile moieties onto the surface of NPs, which can be cleaved in the intra and extracellular environments of cancer cells, to realize the rapid release of drugs. These bonds include ortho-esters, hydrazine, acetal, cis-acotinyl, etc (Liu et al. 2016). Several DDS pH-responsive nano-drug delivery systems based on dynamic boronic acid/ester transformation have recently gained a lot of interest (Cao et al. 2019). Owing to multifunctional characteristics, boronic acid is widely used in the fields of biomedicine, biosensors, chromatographic separation of saccharides, and drug delivery systems (Wang et al. 2013). In aqueous solutions, when the pH is higher than the pKa of boronic acid, this leads to the formation of boronic ester, which is promoted by its strong affinity with diols (Ren et al. 2013). Ester formation is reversible, and it dissociates when the pH is lower than the pKa of boronic acid (Elshaarani et al. 2018). This particular characteristic of boronic acid is critical for the development of pH-responsive nanoformulations. Bearing such captivating characteristics, PBA coated nanoparticles were effectively utilized as pH responsive and glucose responsive drug delivery systems for tumour targeting (Wang et al. 2012; Wang et al. 2017). For instance, PBA containing a polymeric framework enables pH responsive delivery of drugs at the tumour site (Li et al. 2014; Chen et al. 2023). Furthermore, PBA etched polymeric frameworks also enable the delivery of insulin against diabetes disease (Huang et al. 2019; Ma et al. 2021). Moreover, PBA coated metal oxide nanoparticles also showed potent pH responsive delivery of drugs against tumours (Hei et al. 2019; Kundu et al. 2019). In another study, pH-responsive PBA-coated MSN also showed potent activity against tumours (Chen et al. 2018).

Rosmarinic acid (ROS) belongs to a polyphenolic class of compounds originating from the rosemary plant in the Lamiaceae family. ROS possess a variety of biological activities, including anticancer, anti-inflammatory, antimicrobial, antidiabetic, and antiparasitic (Liao et al. 2020). Jin et al. (Jin et al. 2020) reported the potential of ROS in inhibiting Hep-G2 cells by modulating apoptosis, suppressing cell migration, and facilitating caspase activation. Another study reflects the potential of ROS acid in reversing the resistance of lung cancer cells against cisplatin (Liao et al. 2020). However, the poor aqueous solubility and non-specificity of ROS restrict their chemotherapeutic efficacy. To counter that, ROS were conjugated with nanoparticles that enhanced the therapeutic efficacy of ROS, possibly through conjugation with gold nanoparticles, which enhanced its efficacy against breast cancer cells (Ferreira-Gonçalves et al. 2022). Another study shows that the association of ROS with silk fibroin nanoparticles enhances its efficacy against HeLa and MCF-7 cells (Fuster et al. 2021). To date, no pH-responsive formulation of ROS has been reported to highlight its increased therapeutic efficacy against lung or liver cancer.

Till now, numerous PBA based polymeric and metal oxide nanoparticles have served as pH responsive and glucose responsive carriers to enhance the therapeutic efficacy of drugs against tumours and other diseases; however, many obstacles need to be addressed for the clinical application of these carriers, such as poor responsiveness in tumour environments at low pH and poor biocompatibility. To combat this, in this study, for the first time, lignin (LIG)-coated PBA based pH responsive nanoparticles loaded with the phenolic anticancer compound ROS (i.e. LIG-ROS-BMSN) were developed. LIG and ROS were blended together within a PBA mesoporous nanoparticle based framework with aim of stimulating the pH responsive release of ROS under mildly acidic conditions. The functionalized LIG serves as a gatekeeper to prevent drug leakage as well as a colloidal stability and biocompatibility enhancer due to the abundant cathecol and other phenolic groups within its skeleton. Our developed LIG-ROS-BMSN was investigated for its ability to release drug. *The in vitro* cytotoxic activity of our designed pH-responsive BCD-QUE-BZMSN against Hep-G2 and NCI-H460 cells was also evaluated to observe the potential for application against cancer cells.

2. Method and materials

2.1. Materials

All solvents used in our experiments were HPLC-grade and obtained from Fisher Scientific, UK, through a local supplier. Dicyclohexyl carbodiimide (DCC), 4-dimethyl aminopyridine (DMAP), ammonium hydroxide (NH_4OH), Phenyl boronic acid (PBA), 3-aminopropyl silane (APT), Cetyl trimethyl ammonium bromide (CTAB), Tween 80 and ROS were purchased from Sigma Aldrich through a local supplier.

2.2. Methods

2.2.1. Preparation of MSNs, APT-MSNs, and B-MSNs

To achieve solid MSNs, Stober method was used (Liu et al. 2016). In brief, CTAB (1.0 g) was dissolved in a tertiary mixture of ethanol, water, and ammonia (20:100:5), followed by stirring for 30 min at 60 °C. Then, TEOS (10 ml) was added and the mixture was stirred continuously for 4 h, until the solution was turned from opaque to white during the course of reaction. The precipitated material was collected by passing the liquid through a filter paper, and the collected solid product was dispersed in methanolic HCl (10%) and allowed to reflux for 10 h to facilitate the removal of CTAB, followed by washing three times with DI water. To prepare APT-MSN, APTES (0.6 g) was introduced in ACN and stirred until complete homogenization was achieved. Then, HMSNs (200 mg) were added to the homogenised solution of APTES and the resultant suspension was stirred for 4 h to ensure complete functionalization. After 4 h, the APT-MSN suspension was centrifuged and washed with ACN to remove the unreacted APTES. The grafting of boronic acid onto the surface of APT-MSN involves the carbodimide coupling procedure. CBPA (100 mg) was dissolved in DMF and introduced in a 50ml round bottom flask. After ensuring complete homogenization, DCC (600 mg) and DMAP (100 mg) were added to the solution and allowed to stir for 10 min to facilitate carbodimide interaction. Afterward, APT-MSN (200 mg) was added and the mixture was stirred for 24 h at 60 °C. The obtained (B-MSN) was sufficiently rinsed with methanol to remove unreacted constituents and dried for further use.

2.2.2. Synthesis of ROS-B-MSN and LIG-ROS-BMSN

The ROS loading within the pores B-MSN was accomplished using a passive drug loading procedure (Akbar et al. 2021). ROS (1-2 mg/mL) solutions were mixed with the fixed concentration of B-MSN (1 mg/mL) and stirred for 24 h to facilitate maximum drug uptake. After 24 h the drug-loaded (ROS-B-MSN) were centrifuged and the solid product was rinsed with DW and dried in a vacuum. To achieve the LIG capping onto the surface of ROS-B-MSN, ROS-B-MSN (100 mg) was added in water and the pH of the suspension was adjusted to 9. Then, LIG was added to achieve a ratio of 5:1 w/w between ROS-B-MSN and LIG, followed by stirring for 4 h to facilitate complexation between boronic acid and catechol moieties present in LIG. The postsynthetic method involves rinsing

with a sufficient quantity of DI water to remove the unreacted lignin, followed by drying for further use.

2.2.3. Size, zeta potential, and polydispersity index (PDI)

The average hydrodynamic diameter, Zeta potential, and PDI of APT-MSN, B-MSN, ROS-B-MSN, and LIG-ROS-BMSN were obtained by Zetasizer (Zetasizer Nano ZS90 Malvern Instruments, Malvern, UK). In brief, the nanosuspensions were added to a plastic cuvette with care to avoid formation of air bubbles. The cuvette was then placed on a spectrometer and analysis was conducted under ambient conditions. The pressure, refractive index, and medium viscosity were fixed at 80.4, 1.33, and 1.0, respectively. The zeta potential dip cell was used under aforementioned conditions and samples concentrations.

2.2.4. SEM-EDX analysis

The prepared nanoparticles were characterized for their morphology and chemical composition using SEM (Thermo Apero 2 C Lo Vac, Thermo fisher scientific U.S.A) coupled with energy-dispersive X-rays for elemental analysis. The diluted sample was first mounted on silica wafers and the analysis was performed in a scattering mode.

2.2.5. Entrapment efficiency determination

The entrapment efficiency of ROS in ROS-B-MSN was determined by adapting a previously published procedure (Date et al. 2011; Katara and Sachdeva 2019). The obtained ROS-B-MSN were centrifuged at 12,000 rpm for 10 min to separate ROS-BA-MSN. The supernatant containing the free drug was analyzed after serial dilutions at 320 nm on a UV-VIS spectrophotometer. The percentage drug was calculated using the following relation:

$$\%\ \text{Drug Entrapment} = \frac{\text{Amount of drug used} - \text{unloaded drug}}{\text{amount of drug used}} \times 100$$

2.2.6. pH-dependent drug release profiles

The kinetics of drug release in respective buffer solutions were analyzed using the dialysis method as previously reported (Abdelnasir et al. 2020). To sum up, 10 mg of LIG-ROS-BMSN was mixed with 5 ml of buffer (5 ml; pH 5.0 and pH 6.9) that had 1.0% Tween 80 in it. The mixture was then put into the dialysis bags and secured at both ends. The loaded dialysis bag was then immersed in a flask containing 50 ml of buffer (pH 5.0 and pH 6.9), followed by shaking at 100 rpm at 37 °C. At specific intervals, a volume of 2 ml was drawn from each flask and replaced with fresh buffer, and the ROS release was quantified at 320 nm using a UV-VIS spectrometer (Shimadzu 1800 series, Shimadzu Japan). The analysis was performed in triplicate and the data was reported in terms of means and SEM values.

2.2.7. Cell culture

Hep-G2 (Human hepatocarcinoma) and NCI-H460 (Nonsmall cell lung cancer) cell lines were purchased from American Type Culture Collection (ATCC, USA). Cells were cultured in the medium (Hep-G2: Eagle's Minimum Essential Medium; NCI-H460: modified RPMI-1640), supplemented with 10% fetal bovine serum (FBS) using 75 cc sterile tissue culture flask (Corning, United States). The medium was refreshed every 2–3 days per week. At 80% confluency, cells were trypsinized and subcultured as per the guidelines of the manufacturer. Passage numbers (1–5) were used for the mechanistic study of test samples. All tested samples of solutions (*i.e.* ROS, LIG-BMSN, and LIG-ROS-BMSN) were prepared by using DMSO as a solvent.

2.2.8. Cytotoxicity evaluation of LIG-BMSN, ROS, and LIG-ROS-BMSN

The *in vitro* anticancer activity of ROS, LIG-BMSN, and LIG-ROS-BMSN was investigated using human carcinoma cell lines (*i.e.* Hep-G2 and NCI-H460) *via* a gold standard cellular metabolic MTT assay according to the published protocol of Jahan et al. (Jahan-Abad et al. 2017). Briefly, Hep-G2 (7×10^4) and NCI-H460 (5×10^4) cells per well were plated in a sterile tissue culture 96-well microplates (Nest, USA) in triplicate, and kept at 37 °C in 5% CO_2 atmosphere overnight. Next, the culture plate medium was loaded with the test compounds at a series of 0.9, 1.8, 7.5, 15, and 30 μg/mL concentrations, and was reincubated at similar conditions for 24 h. Subsequently, cells were exposed to 0.5 mg/mL of MTT solution (Waltham, USA) for 4 h. The optical absorption (OD) of all treated and untreated groups was measured at 570 nm *using a* microplate reader (Varioskan Microplate Reader, Thermo Fisher Scientific, USA). The anticancer activity was quantified based on survival of exposed Hep-G2 and NCI-H60 with test samples, as compared with the untreated control group. All groups were tested in three individual experiments. The percent cell inhibition *through treatment* with test samples was quantified using the following formula:

$$\%\ \text{Inhibition} = 100 - (\text{Absorbance of test compound} - \text{Absorbance of blank}) / (\text{Absorbance of control} - \text{Absorbance of blank}) \times 100$$

Test samples with anticancer potential were further evaluated for half maximum inhibitory concentration (IC_{50}), using the EZ Fit Enzyme Kinetic programme (Perella Scientific Inc, USA). Identification of the anticancer potential of all tested compounds was performed in three independent experiments ($n = 3$).

2.2.9. Evaluation of cellular morphology via inverted microscopy

To evaluate the morphology of the human Hep-G2 and NCI-H460, cells were seeded in a 6-well tissue culture plate in a similar culture medium and kept for 24 h at 37 °C in a 5% CO_2 atmosphere overnight to allow cell adhesion. Subsequently, cells were incubated with compounds IC_{50} value (Hep-G2 cells: 14.0 ± 0.70 μg/mL ROS, and 1.7 ± 0.01 μg/mL LIG-ROS-BMSN; NCI-H460 cells: 29.10 ± 0.25 μg/mL ROS, and 3.25 ± 0.14 μg/mL LIG-ROS-BMSN) for 24 h. The morphology of cells was observed under an inverted microscope (Nikon E200, Tokyo, Japan), equipped with a digital camera.

3. Result and discussion

3.1. Preparation of MSNs, APT-MSNs, and B-MSNs

The synthetic schematic representation of our nanoparticles is depicted in Figure 1. For synthesis of MSNs,the Stober method was preferred. It involves hydrolysis of orthosilicate and fusion taking place in the presence of a surfactant, which can be removed after the reactions are completed, forming a porous structure (Wu et al. 2013). FTIR analysis of our developed MSNs shows the corresponding peak of OH (stretching and bending) around 3335 cm^{-1} and 1640 cm^{-1} (Figure 2), as well as the corresponding peak of Si-O stretching peak, which appeared at 1173 cm^{-1} and 1043 cm^{-1} which complies with our published findings (Akbar et al. 2021). When APTES was coated onto the

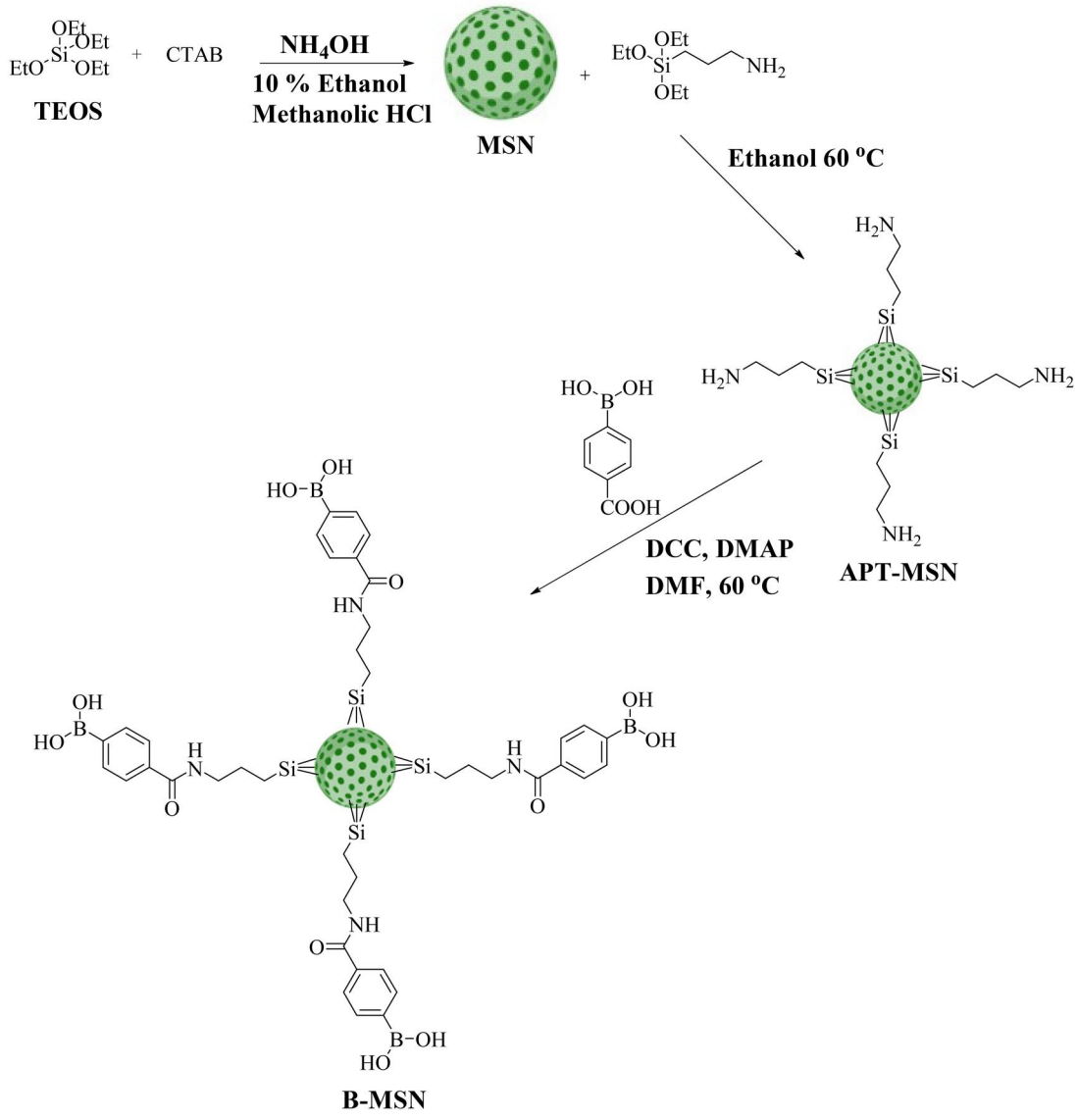

Figure 1. Synthetic scheme for the preparation of B-MSN.

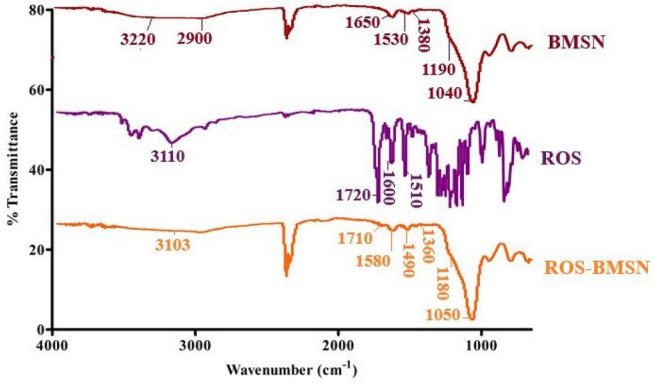

Figure 2. FTIR spectra of B-MSN, ROS and ROS-BMSN.

surface of MSN, the peak stretching and bending frequencies of amine appeared at 3253 and 1630 cm^{-1} along with the C-H stretching at 2943 cm^{-1} consolidating the synthesis of APT-MSN (Oliveira et al. 2017). The final step in nanoparticle synthesis involves the fabrication of a responsive stalk onto the surface of MSNs and for that, 4-CPBA was used and a carbodimide coupling process was used to achieve our desired B-MSNs. FTIR analysis of our developed B-MSN shows an amide (C=O) peak at 1650 cm^{-1},accompanying (C=C) stretching at 1530 cm^{-1} (Figure 2). Furthermore, the peak 1380 cm^{-1} corresponds to B-O stretching (Shi et al. 2017), and Si-O stretching vibrations appeared at 1190 cm^{-1} and 1040 cm^{-1} demonstrating the coating of BA onto the surface of APT-MSN.

3.2. Synthesis of ROS-B-MSN and LIG-ROS-BMSN

The entrapment of ROS within B-MSN was done with aid of the passive diffusion technique. FTIR analysis was conducted to analyze the possible entrapment of ROS within B-MSN. ROS shows the stretching frequency of OH and C=O to be around 3110 cm^{-1} and 1720 cm^{-1}, respectively. Moreover, C=C and O-H bending vibrations also appeared at 1600 cm^{-1} and 1530 cm^{-1}, respectively (Figure 2). When loaded onto B-MSN, FTIR frequencies of ROS varied slightly, for instance, the peak of OH was shifted from 3110 cm^{-1} to 3103 cm^{-1} and the peak of C=O was shifted from 1720 cm^{-1} to 1710 cm^{-1}. In addition, the peak of C=C was varied from 1600 cm^{-1} to 1580 cm^{-1} indicating that ROS is loaded within the pores of B-MSN *via* secondary interaction with OH, C=O, and

C=C groups. The final step involves the formation of a boronate ester between our coated phenylboronic acid and LIG, which provides the maximum pore capping and minimises drug leakage at physiological pH. Lignin (LIG) is generally recognized as a polyaromatic macromolecular compound rich in catechol moieties which under basic medium (pH 9) became negatively charged, thereby interacted with the boron acid moiety and formed boronic ester which is reversible under acidic conditions (Nakahata et al. 2014; Ralph et al. 2019). FTIR spectra of LIG showed OH stretching and bending vibration around 3220 cm^{-1} and 1621 cm^{-1}, respectively (Figure 3). Furthermore, the aliphatic C-H and C=C aromatic stretching also appeared at 2900 cm^{-1} and 1480 cm^{-1} which is in agreement with previously published studies (Derkacheva and Sukhov 2008). When LIG was engineered onto the surface of ROS-BMSN, the peaks of lignin appeared at 3389 cm^{-1}, 2930 cm^{-1}, 1630 cm^{-1}, and 1530 cm^{-1} corresponding to OH (stretching), C-H (stretching), OH (bending), and C=C (stretching) designates the existence of our desired LIG-ROS-BMSN.

3.3. Size distribution and zeta potential investigations

The main attribute of nano drug delivery systems is their high surface-to-volume ratio, which may be accomplished by shrinking the size of nanostructures (Pan et al. 2022). The hydrodynamic diameter of B-MSN was found to be 309.1 ± 25.5 nm. After ROS adsorption (i.e. ROS-B-MSN), the average diameter was decreased to 292 ± 19.3 nm. When the LIG was added to the drug-loaded nanovalve (LIG-ROS-BMSN), the size shrunk even more, by 144.1 ± 0.70 nm. The decrease in size may be due to the coating of hydrophobic ROS and LIG onto the surface of nanoparticles, which reduces aggregation and hence decreases size (Kawish et al. 2020). This idea was supported even more by changing LIG directly on the surface of B-MSNs. The results showed that the LIG-BMSN had a smaller average size, measuring 131.4 ±16.3 nm. The polydispersity index (PDI) determined the colloidal homogeneity of nanoparticles. PDI values lower than 0.5 indicate more colloidal homogeneity (Akbar et al. 2022). In our study, the PDI value

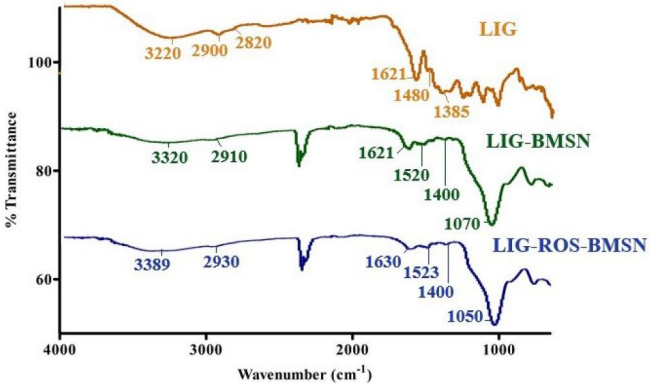

Figure 3. FTIR spectra of LIG, LIG-BMSN and LIG-ROS-BMSN.

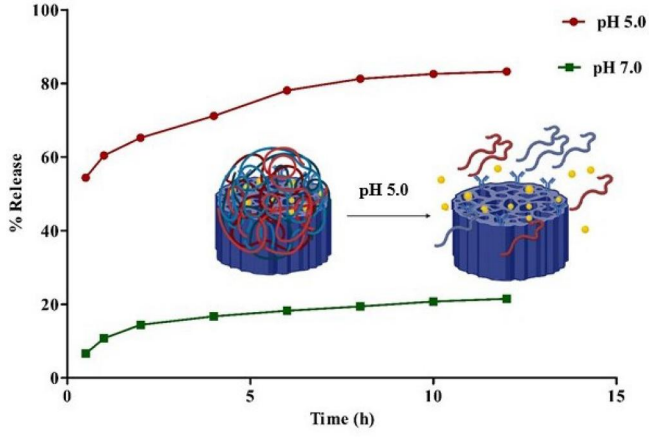

Figure 5. *In vitro* release profile of ROS from LIG-ROS-BMSN at different pH.

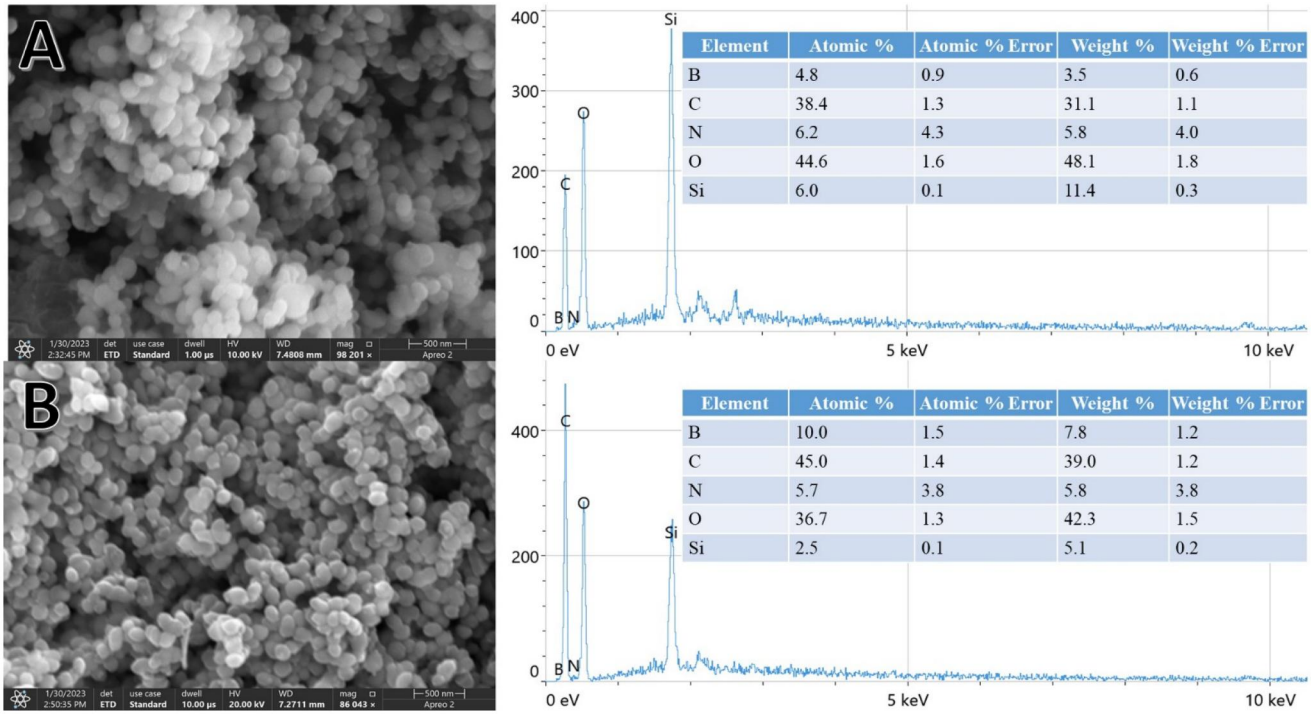

Element	Atomic %	Atomic % Error	Weight %	Weight % Error
B	4.8	0.9	3.5	0.6
C	38.4	1.3	31.1	1.1
N	6.2	4.3	5.8	4.0
O	44.6	1.6	48.1	1.8
Si	6.0	0.1	11.4	0.3

Element	Atomic %	Atomic % Error	Weight %	Weight % Error
B	10.0	1.5	7.8	1.2
C	45.0	1.4	39.0	1.2
N	5.7	3.8	5.8	3.8
O	36.7	1.3	42.3	1.5
Si	2.5	0.1	5.1	0.2

Figure 4. Scanning electron microscopic images of A) B-MSN and B) LIG-ROS-BMSN.

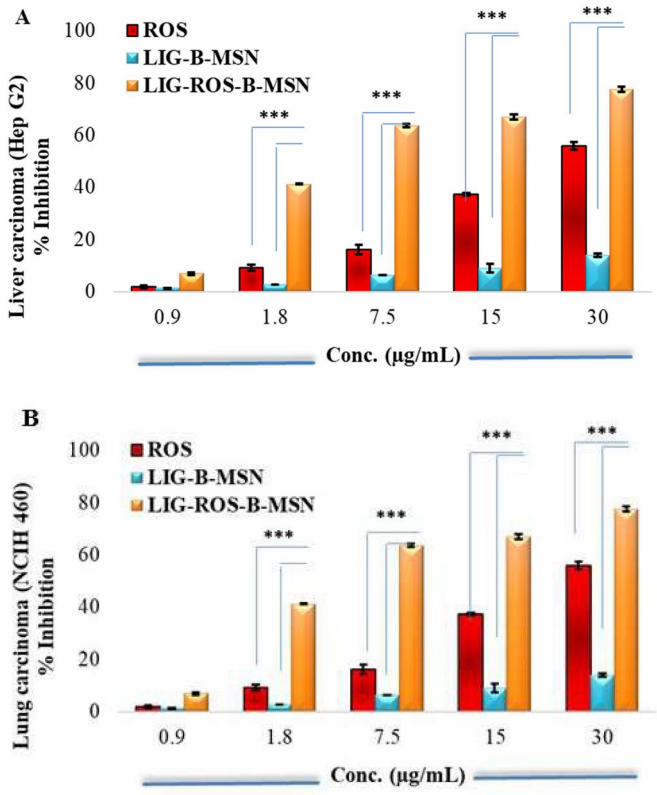

Figure 6. *In vitro* anticancer potential of ROS solution, and its loaded LIG-ROS-BMSN formulation against human hepatocarcinoma (Hep-G2) and (NCI-H460) experimental groups. (A) 24 h Treatment of (Hep-G2) cells with LIG-ROS-BMSN exhibited toxicity at 1.8–30 µg/mL concentrations. (B) 24-h treatment of (NCI-H460) cells with LIG-ROS-BMSN exhibited toxicity at 0.9–30 µg/mL concentrations.

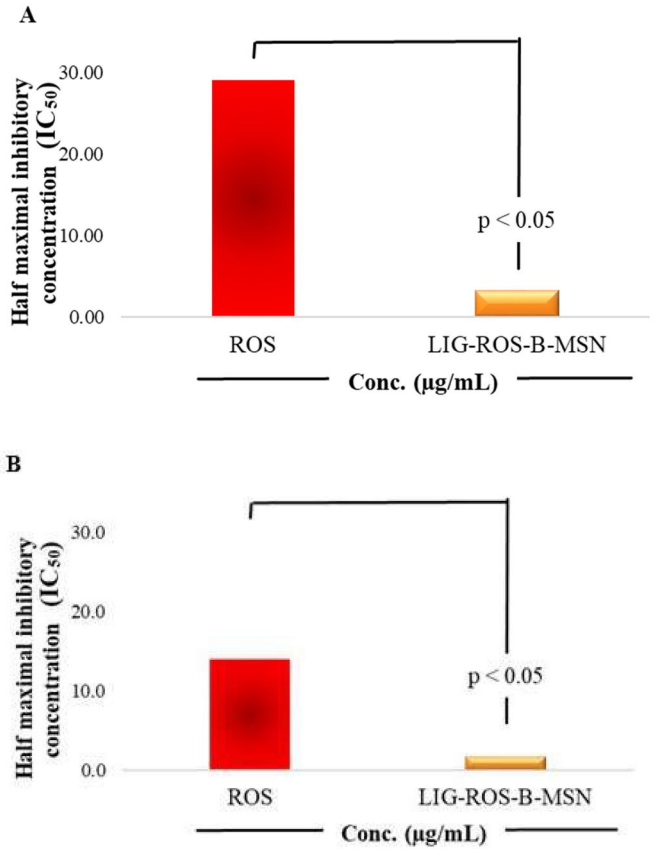

Figure 7. (A) The half-maximal concentration (IC_{50}) of ROS solution and LIG-ROS-BMSN against the human lung carcinoma experimental group was carried out in three individual triplicates ($n = 3$). (B) The half-maximal concentration (IC_{50}) of LIG-ROS-BMSN and ROS solution. Three independent *in vitro* experiments ($n = 3$) in the hepatocytes experiment group were run for the identification of the toxicity profile of tested samples.

of B-MSN, ROS-B-MSN, LIG-BMSN, and LIG-ROS-BMSN were found to be 0.427 ± 0.09, 0.473 ± 0.08, 0.219 ± 0.08 and 0.220 ± 0.03, respectively. The fact that the PDI value went down supports our idea that adding more particles can improve the colloidal performance of the pH-responsive nanovalve. Due to the existence of silanol and Boronic acid moieties, the zeta potential of BZ-MSN was found to be −20.7 ± 1.61 mV. When ROS was loaded into nanoparticle pores (ROS-BMSN), the zeta potential was reduced to −13.1 ± 1.1 mV and the capping of LIG onto the surface of ROS-B-MSN (i.e. LIG-ROS-BMSN) increases the charge intensity to −15.7 ± 0.46 mV. The zeta potential of formulation without the drug (i.e. LIG-BMSN) was found to be −8.97 ± 3.83 mV. The reduction in zeta potential values may reflect the capping to silanol moieties due to entrapment of ROS and LIG onto the pH-activated nano valve.

3.4. SEM-EDX analysis

Scanning electron microscopy (SEM) images revealed that our developed B-MSN and LIG-ROS-BMSN are nearly spherical (Figure 4(A,B)). EDX analysis depicted that there was a wide difference in the elemental composition of developed B-MSN and LIG-ROS-BMSN. In the case of B-MSN, the elemental composition of C (31.1 ± 1.1%), Si (11.4 ± 0.3%), O (48.1 ± 1.8%), B (3.5 ± 0.9%), and N (5.8 ± 4.0%) was observed (Figure 4(A)). However, when ROS was loaded and LIG was capped onto the surface of B-MSN (LIG-ROS-BMSN), the composition varies to C (39.0 ± 1.1%), Si (5.1 ± 0.2%), O (42.3 ± 1.5%), B (7.8 ± 1.2%) and N (5.8 ± 3.8%) (Figure 4(B)) showing the effective loading of ROS and capping of LIG onto the surface of our desired pH-responsive nano valve.

3.5. Drug entrapment efficiency

One of the main objectives of this study was to develop a pH-responsive nano-valve of specified area and pore volume that has to possess a tendency to entrap and deliver a higher amount of therapeutic material at the desired site of action (Mohseni et al. 2015). Passive drug loading procedure was adopted to enhance the entrapment of the drug within the pores of B-MSN. The entrapment process was progressed at a varied concentration of ROS (0.5–1 mg/ml) and the solvent was chosen based on the higher solubility of ROS to facilitate diffusion within the pores of B-MSN. The outcome indicated that ROS was entrapped within B-MSN in a concentration-dependent manner and entrapment efficiency of as high as 49.3 ± 2.43% was obtained when the drug concentration was 1 mg/mL, compared to 35.8 ± 1.54% when the drug concentration was 0.5 mg/mL. Thus, increasing drug concentration resulted in facilitated drug diffusion and increased entrapment.

3.6. In vitro drug release study

Lignin (LIG) is generally referred to as polyphenolic compounds containing diverse functional groups such as carboxylic acids, phenols, catechols, hydroxides, etc. The previous research suggests that pH-dependent complexation occurs between phenylboronic acid (PBA) and catechol moieties; therefore, a nano valve comprised of PBA-coated mesoporous silica nanoparticles loaded with ROS was constructed in our study. The ROS-B-MSN was

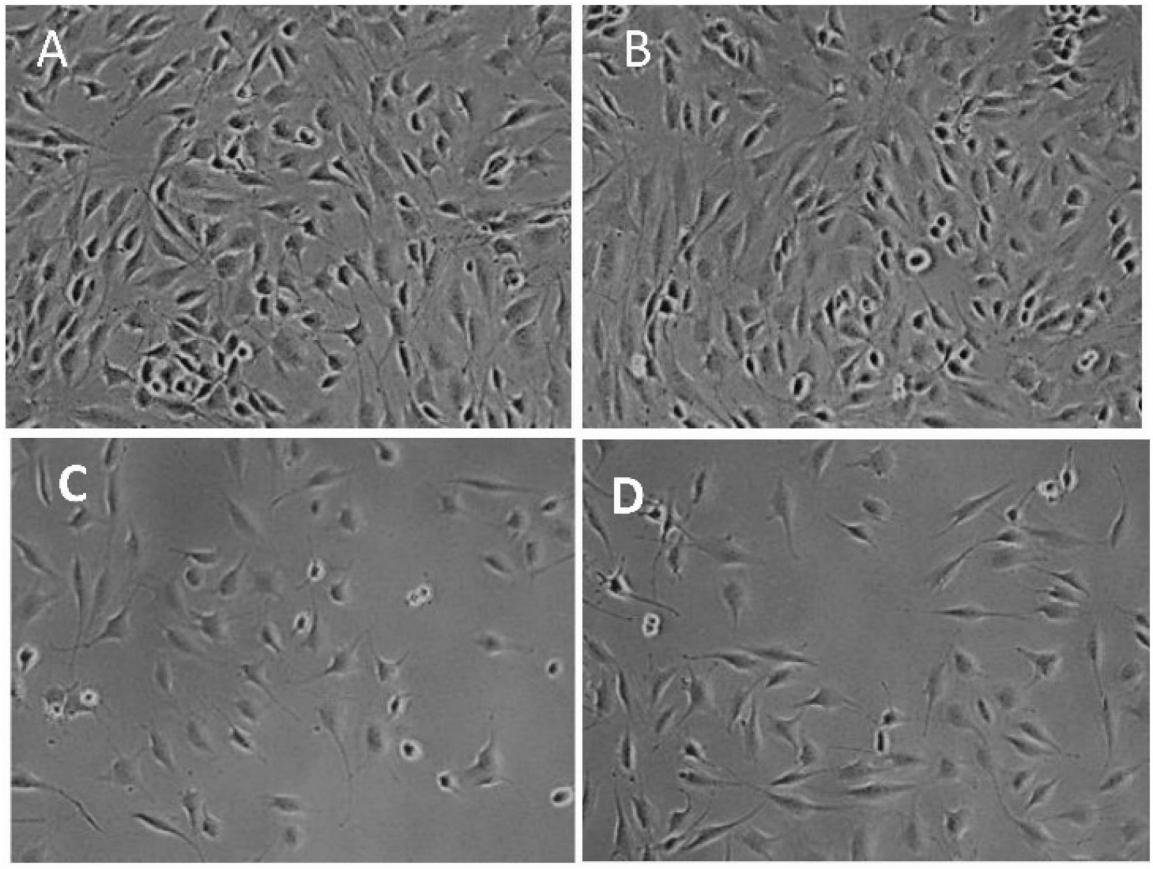

Figure 8. Apoptotic hallmarks in human hepatocarcinoma. Control (A) and nano vesicles-treated (B) Hep-G2 cells displayed high confluency of the monolayer, as compared with the 24 h exposure of 14.0 ± 0.7 μg/mL ROS solution (C), and 1.7 ± 0.01 μg/mL of LIG-ROS-BMSN (D). ROS and its loaded LIG-ROS-BMSN experimental group (C-D) depicted a significant reduction in cell size and cellular networking, as compared to the control. All three independent *in vitro* cellular experiments had shown similar cellular features of Hep-G2 cells.

further coated with LIG, which serves as a pH-responsive gatekeeper for ROS release in cancer cells. To analyze and verify pH-responsive ROS release from the developed LIG-ROS-BMSN, we studied ROS release in PBS (pH 7.4 or 5.0). As depicted in Figure 5, only 19.4% ROS was released from LIG-ROS-BMSN over 12 h at pH 7.4 while nearly 80% ROS was released at pH 5.0 within 12 h, thus, ROS demonstrated accelerated release at pH 5.0. This may be because under mildly acidic conditions, the complexation between PBA moiety and LIG is broken, leading to opening of the nano valve (i.e. pores), and increased ROS release rate (Su et al. 2011; Chen W et al. 2023). Moreover, the release of ROS from LIG-ROS-BMSN follows zero-order kinetics with an R^2 value of 0.9041.

3.7. Cytotoxic effects of LIG-B-MSN, ROS, and LIG-ROS-BMSN

The *in vitro* cytotoxicity of LIG-ROS-BMSN pH-responsive nano valve in delivering chemotherapeutics was analyzed using MTT assay. The vacant LIG-B-MSN nano valve did not show any adverse effect on the tested Hep-G2 and NCI-H460 cell lines at the highest tested concentration of 30 μg/mL (Figure 6(A,B)), respectively. This comes in agreement with a previous report, highlighting the biocompatibility of mesoporous silica nanoparticles (Meng et al. 2010; Kong et al. 2019) and suggesting that our developed nano valve is suitable as a pH-responsive drug delivery system. Treatment of ROS against Hep-G2 and NCI-H460 cell lines causes 56 ± 1.55% loss in cell viability against both cell lines (Figure 6(A,B)) at the highest concentration of 30 μg/mL. The IC_{50} value of ROS against both Hep-G2 and NCI-H460 cell lines was found to be 14.0 ± 0.7 μg/mL and 29.10 ± 0.25 μg/mL, as presented in Figure 7(A,B) respectively. The greater IC_{50} values of ROS against both tested cell lines may be due to the hydrophobic nature of ROS, which restricts the diffusion of the drug across the cellular membrane and hence lowers the cytotoxic effect (Hakemi et al. 2021). Treatment of human cancer cell lines, Hep-G2 and NCI-H460, against the pH-responsive LIG-ROS-BMSN nano valve causes substantially greater losses in cell viability (77.4 ± 1.0%) at the concentration of 30 μg/mL for Hep-G2 and NCI-H460 cell lines compared to ROS, as depicted in (Figure 6(A,B)). Furthermore, IC_{50} value against both cell lines were found to be 1.70 ± 0.01 μg/mL and 3.25 ± 0.14 μg/mL, respectively. The mechanism of cellular damage of the designed LIG-ROS-BMSN at potentially lower IC_{50} values is likely to be linked with the enhanced endocytosis of our pH-responsive LIG-ROS-BMSN nano valve across the cellular membrane and therefore triggers the drug release in an endosomal compartment, which as consequence modulates apoptosis, suppresses cell migration, and facilitates caspase activation, which cause significant cytotoxic effects (Meng et al. 2010). The substantial cytotoxicity of pH-responsive LIG-ROS-BMSN nano valve suggests that this delivery system can potentially be used for effective targeting of human liver and lung cancers.

3.8. Evaluation of cellular morphology via inverted microscopy

Hep-G2 cells were exposed to the IC_{50} values of ROS solution and LIG-ROS-BMSN nanovalve for 24 h. They showed the typical morphological hallmarks of apoptosis. The study of Elmore S. (2007)

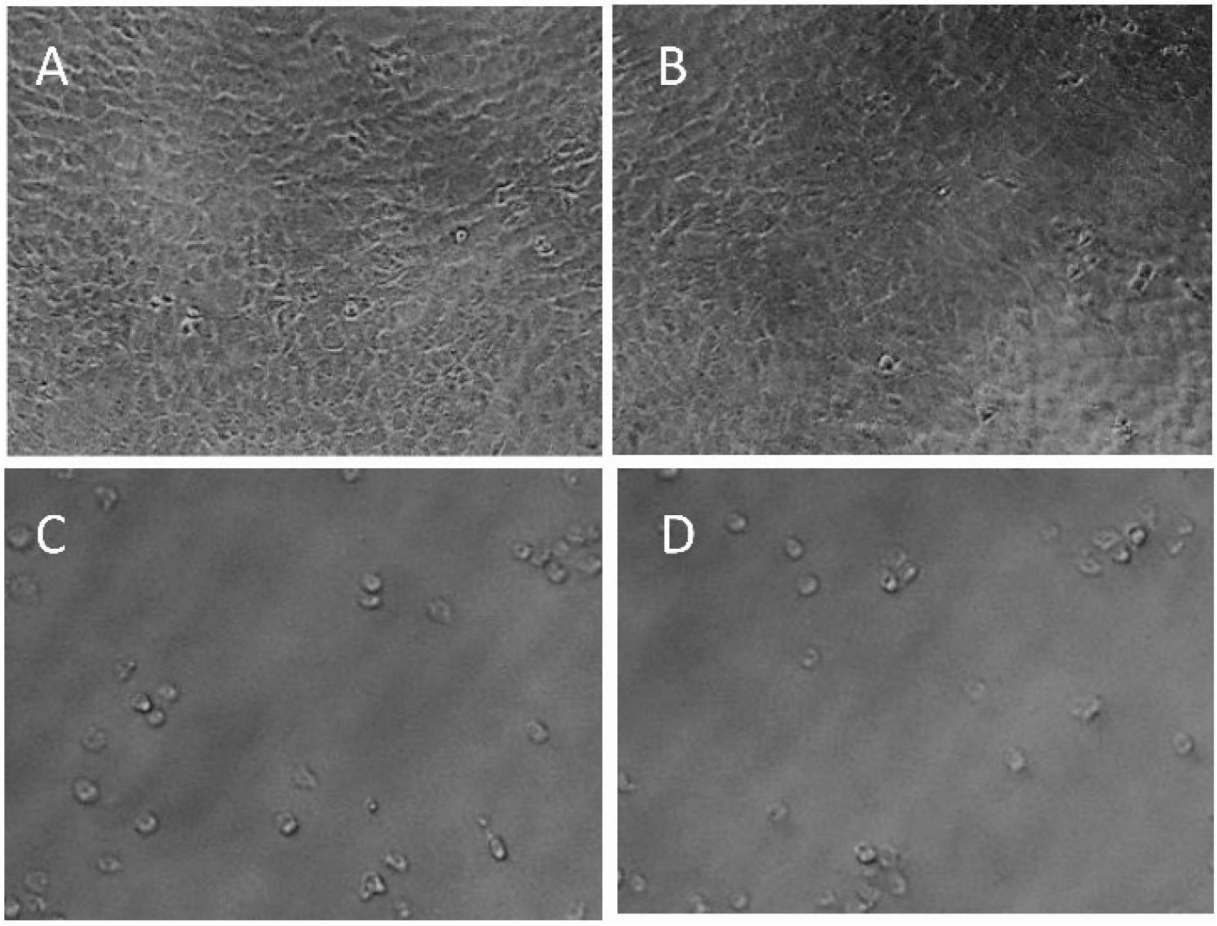

Figure 9. Apoptotic hallmarks in non-small-cell lung cancer. Control (a), (B) nano vesicles-treated, NCI-H460 cells displayed high confluency, as compared with the 24 h exposure of 29.10 ± 0.25 μg/mL quercetin (C), and 3.25 ± 0.14 μg/mL of LIG-ROS-BMSN (D). ROS and its loaded LIG-ROS-BMSN experimental group (C-D) depicted a significant inhibition in cell proliferation and adhesion, and caused round morphology, as compared to untreated cells (a).

characterized apoptosis by reducing cell volume, cell shrinkage, decreased chromatin condensation, and progression of cytoplasmic blebs (Susan Elmore) that were also identified in our *in vitro* treated experimental group. (Figure 8(A)) displayed high confluency of monolayer Hep-G2 cells in *in vitro* untreated cellular group. However, cells exposed to ROS (IC_{50}: 14.0 ± 0.7 μg/mL ROS), and LIG-ROS-BMSN nano-vesicles (IC_{50}: 1.7 ± 0.01 μg/mL) halted cell proliferation, and thus, inhibited cellular networking, as compared to untreated Hep-G2 cells (Figure 8). Similarly, NCI-H460 lung carcinoma treated with their IC_{50} value (29.10 ± 0.25 μg/mL ROS, and the 3.425 ± 0.1 μg/mL and LIG-ROS-BMSN nano-valve caused a reduction in cell adhesion and proliferation, and exhibited a spherical morphology of lung cells, compared to untreated cells (Figure 9).

4. Conclusion

We have successfully conceptualized and designed LIG-capped phenylboronic acid containing pH-responsive nano-valve (B-MSN) for delivery of ROS across lung and liver cells *in vitro*. LIG-ROS-BMSN had a nanoscale size, spherical morphology and they revealed high drug entrapment efficiencies. The presence of boronic acid on the surface of NPs facilitates ROS release under mildly acidic conditions. The enhanced chemotherapeutic potential of our developed LIG-ROS-BMSN formulation against Hep-G2 and NCI-H460 is evident from its lower IC_{50} values as compared to ROS alone. This significant cytotoxic effects of the developed LIG-ROS-BMSN at lower IC_{50} values is due to higher internalization of our nano valve within the cell, and facilitates ROS release at endosomal pH and implies that our LIG-ROS-BMSN can be viable chemotherapeutic formulation of ROS against both lung and liver cancer cells.

Acknowledgments

The authors would like to thank H.E.J Research Institute of Chemistry University of Karachi and Higher Education Commission for funding and support.

Credit authorship contribution statement

Muhammad Kawish: Conceptualization, Data curation, Formal analysis, Investigation, Methodology, writing (original draft), review, and editing. **Nimra Naz Siddiqui:** *In vitro* cellular experiments. **Abdelbary Elhissi**, **Humera Jahan:** Methodology and manuscript review. **Hina Zahid:** Writing – review & editing. **Bushra khatoon:** Methodology. **Muhammad Raza Shah:** Methodology, Project administration, Resources, Software, Supervision, Validation, Visualization, Writing – review & editing.

Disclosure statement

The author(s) reported no potential conflicts of interest.

Funding

The author(s) reported there is no funding associated with the work featured in this article.

References

Abdelnasir S, Anwar A, Kawish M, Anwar A, Raza M, Siddiqui R, Khan N. 2020. Metronidazole conjugated magnetic nanoparticles loaded with amphotericin B exhibited potent effects against pathogenic Acanthamoeba castellanii belonging to the T4 genotype. AMB Express. 10(1):127. doi:10.1186/s13568-020-01061-z.

Akbar N, Kawish M, Jabri T, Khan NA, Shah MR, Siddiqui R. 2021. Enhancing efficacy of existing antibacterials against selected multiple drug resistant bacteria using cinnamic acid-coated magnetic iron oxide and mesoporous silica nanoparticles. Pathog Glob Health. 116(7):438–454. doi:10.1080/20477724.2021.2014235.

Akbar N, Kawish M, Khan NA, Shah MR, Alharbi AM, Alfahemi H, Siddiqui R. 2022. Hesperidin-, curcumin-, and amphotericin B-based nano-formulations as potential antibacterials. Antibiotics. 11(5):696. doi:10.3390/antibiotics11050696.

Cao J, Gao X, Cheng M, Niu X, Li X, Zhang Y, Liu Y, Wang W, Yuan Z. 2019. Reversible shielding between dual ligands for enhanced tumor accumulation of ZnPc-loaded micelles. Nano Lett. 19(3):1665–1674. doi:10.1021/acs.nanolett.8b04645.

Chan MH, Lin HM. 2015. Preparation and identification of multifunctional mesoporous silica nanoparticles for in vitro and in vivo dual-mode imaging, theranostics, and targeted tracking. Biomaterials. 46:149–158. doi:10.1016/j.biomaterials.2014.12.034.

Chen H, Kuang Y, Liu R, Chen Z, Jiang B, Sun Z, Chen X, Li C. 2018. Dual-pH-sensitive mesoporous silica nanoparticle-based drug delivery system for tumor-triggered intracellular drug release. J Mater Sci. 53(15):10653–10665. doi:10.1007/s10853-018-2363-8.

Chen W, Xie W, Zhao G, Shuai Q. 2023. Efficient pH-responsive nano-drug delivery system based on dynamic boronic acid/ester transformation. Molecules. 28(11):4461. doi:10.3390/molecules28114461.

Cheng W, Nie J, Xu L, Liang C, Peng Y, Liu G, Wang T, Mei L, Huang L, Zeng X. 2017. pH-Sensitive delivery vehicle based on folic acid-conjugated polydopamine-modified mesoporous silica nanoparticles for targeted cancer therapy. ACS Appl Mater Interfaces. 9(22):18462–18473. doi:10.1021/acsami.7b02457.

Date AA, Nagarsenker MS, Patere S, Dhawan V, Gude R, Hassan P, Aswal V, Steiniger F, Thamm J, Fahr A. 2011. Lecithin-based novel cationic nanocarriers (Leciplex) II: improving therapeutic efficacy of quercetin on oral administration. Mol Pharm. 8(3):716–726. doi:10.1021/mp100305h.

Derkacheva O, Sukhov D. 2008. Investigation of lignins by FTIR spectroscopy. Macromolecular Symposia. 265(1):61–68.

Elsabahy M, Heo GS, Lim SM, Sun G, Wooley KL. 2015. Polymeric nanostructures for imaging and therapy. Chem Rev. 115(19):10967–11011. doi:10.1021/acs.chemrev.5b00135.

Elsabahy M, Wooley KL. 2015. Data mining as a guide for the construction of cross-linked nanoparticles with low immunotoxicity via control of polymer chemistry and supramolecular assembly. Acc Chem Res. 48(6):1620–1630. doi:10.1021/acs.accounts.5b00066.

Elshaarani, Tarig, Yu, Haojie, Wang, Li, Ullah, Raja Summe, Haroon, Muhammad, Khan, Rizwan Ullah, Fahad, Shah, Khan, Amin, Nazir, Ahsan, Usman, Muhammad, Naveed, Kaleem-Ur-Rahman, 2018. Synthesis of hydrogel-bearing phenylboronic acid moieties and their applications in glucose sensing and insulin delivery. J Mater Chem B. 6(23):3831–3854. doi:10.1039/c7tb03332j.

Ferreira-Gonçalves T, Gaspar MM, Coelho JMP, Marques V, Viana AS, Ascensão L, Carvalho L, Rodrigues CMP, Ferreira HA, Ferreira D, et al. 2022. The role of rosmarinic acid on the bioproduction of gold nanoparticles as part of a photothermal approach for breast cancer treatment. Biomolecules. 12(1):71. doi:10.3390/biom12010071.

Fuster MG, Carissimi G, Montalbán MG, Víllora G. 2021. Antitumor activity of rosmarinic acid-loaded silk fibroin nanoparticles on HeLa and MCF-7 cells. Polymers (Basel). 13(18):3169. doi:10.3390/polym13183169.

Hakemi P, Ghadi A, Mahjoub S, Zabihi E, Tashakkorian H. 2021. Fabrication of PCL-PEG-PCL nanocarrier for Co-loading of docetaxel/quercetin and assessment of its effect on growth inhibition of human liver cancer (Hep-G2) cell line. International Journal of Nano Dimension. 12(4):355–368.

Hei M, Wu H, Fu Y, Xu Y, Zhu W. 2019. Phenylboronic acid functionalized silica nanoparticles with enlarged ordered mesopores for efficient insulin loading and controlled release. J Drug Delivery Sci Technol. 51:320–326. doi:10.1016/j.jddst.2019.03.031.

Huang Q, Wang L, Yu H, Ur-Rahman K. 2019. Advances in phenylboronic acid-based closed-loop smart drug delivery system for diabetic therapy. J Control Release. 305:50–64. doi:10.1016/j.jconrel.2019.05.029.

Jahan-Abad AJ, Morteza-Zadeh P, Negah SS, Gorji A. 2017. Curcumin attenuates harmful effects of arsenic on neural stem/progenitor cells. Avicenna Journal of Phytomedicine. 7(4):376.

Jin B, Liu J, Gao D, Xu Y, He L, Zang Y, Li N, Lin D. 2020. Detailed studies on the anticancer action of rosmarinic acid in human Hep-G2 liver carcinoma cells: evaluating its effects on cellular apoptosis, caspase activation and suppression of cell migration and invasion. Journal of BUON: official Journal of the Balkan Union of Oncology. 25(3):1383–1389. eng.

Katara R, Sachdeva S. 2019. Design, characterization, and evaluation of aceclofenac-loaded Eudragit RS 100 nanoparticulate system for ocular delivery. Pharmaceutical Development and Technology. 24(3):368–379.

Kawish M, Elhissi A, Jabri T, Muhammad Iqbal K, Zahid H, Shah MR. 2020. Enhancement in oral absorption of ceftriaxone by highly functionalized magnetic iron oxide nanoparticles. Pharmaceutics. 12(6):492. doi:10.3390/pharmaceutics12060492.

Kinoh H, Miura Y, Chida T, Liu X, Mizuno K, Fukushima S, Morodomi Y, Nishiyama N, Cabral H, Kataoka K. 2016. Nanomedicines eradicating cancer stem-like cells in vivo by pH-triggered intracellular cooperative action of loaded drugs. ACS Nano. 10(6):5643–5655. doi:10.1021/acsnano.6b00900.

Kong Z-L, Kuo H-P, Johnson A, Wu L-C, Chang KLB. 2019. Curcumin-loaded mesoporous silica nanoparticles markedly enhanced cytotoxicity in hepatocellular carcinoma cells. Int J Mol Sci. 20(12):2918. doi:10.3390/ijms20122918.

Kundu M, Sadhukhan P, Ghosh N, Chatterjee S, Manna P, Das J, Sil PC. 2019. pH-responsive and targeted delivery of curcumin via phenylboronic acid-functionalized ZnO nanoparticles for breast cancer therapy. J Adv Res. 18:161–172. doi:10.1016/j.jare.2019.02.036.

Lavan DA, McGuire T, Langer R. 2003. Small-scale systems for in vivo drug delivery. Nat Biotechnol. 21(10):1184–1191. doi:10.1038/nbt876.

Li L, Zeng Z, Chen Z, Gao R, Pan L, Deng J, Ye X, Zhang J, Zhang S, Mei C, et al. 2020. Microenvironment-triggered degradable

hydrogel for imaging diagnosis and combined treatment of intraocular choroidal melanoma. ACS Nano. 14(11):15403–15416. doi:10.1021/acsnano.0c06000.

Li S, Hu K, Cao W, Sun Y, Sheng W, Li F, Wu Y, Liang X-J. 2014. pH-responsive biocompatible fluorescent polymer nanoparticles based on phenylboronic acid for intracellular imaging and drug delivery. Nanoscale. 6(22):13701–13709. doi:10.1039/c4nr04054f.

Liao XZ, Gao Y, Sun LL, Liu JH, Chen HR, Yu L, Chen ZZ, Chen WH, Lin LZ. 2020. Rosmarinic acid reverses non-small cell lung cancer cisplatin resistance by activating the MAPK signaling pathway. Phytother Res. 34(5):1142–1153. eng. doi:10.1002/ptr.6584.

Liu J, Liu Q, Yang C, Sun Y, Zhang Y, Huang P, Zhou J, Liu Q, Chu L, Huang F, et al. 2016. cRGD-modified benzimidazole-based pH-responsive nanoparticles for enhanced tumor targeted doxorubicin delivery. ACS Appl Mater Interfaces. 8(17):10726–10736. doi:10.1021/acsami.6b01501.

Liu J, Luo Z, Zhang J, Luo T, Zhou J, Zhao X, Cai K. 2016. Hollow mesoporous silica nanoparticles facilitated drug delivery via cascade pH stimuli in tumor microenvironment for tumor therapy. Biomaterials. 83:51–65. doi:10.1016/j.biomaterials.2016.01.008.

Ma Q, Zhao X, Shi A, Wu J. 2021. Bioresponsive functional phenylboronic acid-based delivery system as an emerging platform for diabetic therapy. Int J Nanomedicine. 16(null):297–314. doi:10.2147/IJN.S284357.

Meng H, Xue M, Xia T, Zhao Y-L, Tamanoi F, Stoddart JF, Zink JI, Nel AE. 2010. Autonomous in vitro anticancer drug release from mesoporous silica nanoparticles by pH-sensitive nanovalves. J Am Chem Soc. 132(36):12690–12697. doi:10.1021/ja104501a.

Mohseni M, Gilani K, Mortazavi SA. 2015. Preparation and characterization of rifampin loaded mesoporous silica nanoparticles as a potential system for pulmonary drug delivery. Iranian Journal of Pharmaceutical Research: IJPR. 14(1):27–34. eng.

Nakahata M, Mori S, Takashima Y, Hashidzume A, Yamaguchi H, Harada A. 2014. pH-and sugar-responsive gel assemblies based on boronate–catechol interactions. ACS Macro Lett. 3(4):337–340. doi:10.1021/mz500035w.

Oliveira L, Bouchmella K, Picco AS, Capeletti LB, Gonçalves KA, Santos J, Kobarg J, Cardoso MB. 2017. Tailored silica nanoparticles surface to increase drug load and enhance bactericidal response. J Braz Chem Soc. 28:1715–1724.

Palanikumar L, Al-Hosani S, Kalmouni M, Nguyen VP, Ali L, Pasricha R, Barrera FN, Magzoub M. 2020. pH-responsive high stability polymeric nanoparticles for targeted delivery of anticancer therapeutics. Commun Biol. 3(1):95. doi:10.1038/s42003-020-0817-4.

Pan F, Giovannini G, Zhang S, Altenried S, Zuber F, Chen Q, Boesel LF, Ren Q. 2022. pH-responsive silica nanoparticles for the treatment of skin wound infections. Acta Biomater. 145:172–184. doi:10.1016/j.actbio.2022.04.009.

Petros RA, DeSimone JM. 2010. Strategies in the design of nanoparticles for therapeutic applications. Nat Rev Drug Discov. 9(8):615–627. doi:10.1038/nrd2591.

Ralph J, Lapierre C, Boerjan W. 2019. Lignin structure and its engineering. Curr Opin Biotechnol. 56:240–249. doi:10.1016/j.copbio.2019.02.019.

Ren J, Zhang Y, Zhang J, Gao H, Liu G, Ma R, An Y, Kong D, Shi L. 2013. pH/sugar dual responsive core-cross-linked PIC micelles for enhanced intracellular protein delivery. Biomacromolecules. 14(10):3434–3443. doi:10.1021/bm4007387.

Shi Z, Pu L, Guo Y, Fu Z, Zhao W, Zhu Y, Wu J, Wang F. 2017. Boronic acid-modified magnetic Fe3O4@mTiO2 microspheres for highly sensitive and selective enrichment of n-glycopeptides in amniotic fluid. Sci Rep. 7(1):4603. doi:10.1038/s41598-017-04517-8.

Song Y, Zhu P, Xu Z, Chen J. 2020. Dual-responsive dual-drug-loaded bioinspired polydopamine nanospheres as an efficient therapeutic nanoplatform against drug-resistant cancer cells. ACS Appl Bio Mater. 3(9):5730–5740. doi:10.1021/acsabm.0c00512.

Su J, Chen F, Cryns VL, Messersmith PB. 2011. Catechol polymers for ph-responsive, targeted drug delivery to cancer cells. J Am Chem Soc. 133(31):11850–11853. doi:10.1021/ja203077x.

Torchilin VP. 2014. Multifunctional, stimuli-sensitive nanoparticulate systems for drug delivery. Nat Rev Drug Discov. 13(11):813–827. doi:10.1038/nrd4333.

Volk T, Jähde E, Fortmeyer H, Glüsenkamp K, Rajewsky M. 1993. pH in human tumour xenografts: effect of intravenous administration of glucose. Br J Cancer. 68(3):492–500. doi:10.1038/bjc.1993.375.

Wang B, Yuan T, Zha L, Liu Y, Chen W, Zhang C, Bao Y, Dong Q. 2021. Oral delivery of gambogenic acid by functional polydopamine nanoparticles for targeted tumor therapy. Mol Pharm. 18(3):1470–1479. doi:10.1021/acs.molpharmaceut.1c00030.

Wang J, Lee JS, Kim D, Zhu L. 2017. Exploration of zinc oxide nanoparticles as a multitarget and multifunctional anticancer nanomedicine. ACS Appl Mater Interfaces. 9(46):39971–39984. doi:10.1021/acsami.7b11219.

Wang X, Xia N, Liu L. 2013. Boronic acid-based approach for separation and immobilization of glycoproteins and its application in sensing. Int J Mol Sci. 14(10):20890–20912. doi:10.3390/ijms141020890.

Wang Y, Zhang X, Han Y, Cheng C, Li C. 2012. pH-and glucose-sensitive glycopolymer nanoparticles based on phenylboronic acid for triggered release of insulin. Carbohydr Polym. 89(1):124–131. doi:10.1016/j.carbpol.2012.02.060.

Wu S-H, Mou C-Y, Lin H-P. 2013. Synthesis of mesoporous silica nanoparticles. Chem Soc Rev. 42(9):3862–3875. doi:10.1039/c3cs35405a.

Zhang Y, Cai K, Li C, Guo Q, Chen Q, He X, Liu L, Zhang Y, Lu Y, Chen X, et al. 2018. Macrophage-membrane-coated nanoparticles for tumor-targeted chemotherapy. Nano Lett. 18(3):1908–1915. doi:10.1021/acs.nanolett.7b05263.